Multifractality of entangled random walks and non-uniform hyperbolic spaces

2000 J. Phys. A: Math. Gen. 33 5631

(http://iopscience.iop.org/0305-4470/33/32/302)

J. Phys. A: Math. Gen. **33** (2000) 5631–5652. Printed in the UK PII: S0305-4470(00)11113-8

Multifractality of entangled random walks and non-uniform hyperbolic spaces

Raphael Voituriez† and Sergei Nechaev†‡

† Laboratoire de Physique Théorique et Modèles Statistiques, Université Paris Sud, 91405 Orsay Cedex, France

‡ L D Landau Institute for Theoretical Physics, 117940, Moscow, Russian Federation

Received 19 January 2000

Abstract. Multifractal properties of the distribution of topological invariants for a model of trajectories randomly entangled with a non-symmetric lattice of obstacles are investigated. Using the equivalence of the model to random walks on a locally non-symmetric tree, statistical properties of topological invariants, such as drift and return probabilities, have been studied by means of a renormalization-group (RG) technique. The comparison of the analytical RG results with numerical simulations as well as with the rigorous results of Gerl and Woess demonstrates clearly the validity of our approach. It is shown explicitly, by direct counting for the discrete version of the model and by conformal methods for the continuous version, that multifractality occurs when local uniformity of the phase space (which has an exponentially large number of states) has been broken.

1. Introduction

The phenomenon of multifractality consists of a scale dependence of critical exponents. It has been widely discussed in the literature for a wide range of issues, such as the statistics of strange sets [1], diffusion-limited aggregation [2], wavelet transforms [3], conformal invariance [4] or statistical properties of critical wavefunctions of massless Dirac fermions in a random magnetic field [5–7].

The aim of our work is not only to describe a new model possessing a multiscaling dependence, but also to show that the phenomenon of multifractality is related to local non-uniformity of the exponentially growing ('hyperbolic') underlying 'target' phase space, through an example of an entangled random-walks distribution in homotopy classes. Indeed, to the best of our knowledge, almost all examples of multifractal behaviour for physical [5–7] or more abstract [1, 8] systems share one common feature—all target phase spaces have a hyperbolic structure and are locally non-uniform.

We believe that multiscaling is a much more generic physical phenomenon compared with uniform scaling, appearing when the phase space of a system possesses a hyperbolic structure with local symmetry breaking. Such a perturbation of local symmetry could be either regular or random—from our point of view the details of the origin of local non-uniformity play a less significant role.

We discuss below the basic features of multifractality in a locally non-uniform regular hyperbolic phase space. We show, in particular, that a multifractal behaviour is encountered in statistical topology in the case of an entangled (or knotted) random-walks distribution in topological classes.

0305-4470/00/325631+22$30.00

The paper is organized as follows. In section 2 we consider a two-dimensional (2D) N-step random walk in a non-symmetric array of topological obstacles and investigate the multiscaling properties of the 'target' phase space for a set of specific topological invariants—the 'primitive paths'. The renormalization-group computations of mean length of the primitive path, as well as return probabilities to the unentangled topological state are developed in section 3. Section 4 is devoted to the application of conformal methods to a geometrical analysis of multifractality in locally non-uniform hyperbolic spaces.

2. Multifractality of topological invariants for random entanglements in a lattice of obstacles

The concept of multifractality has been formulated and clearly explained in [1]. We begin by recalling the basic definitions of the Rényi spectrum, which will be used in the following.

Let $\nu(C_i)$ be an abstract invariant distribution characterizing the probability of a dynamical system staying in a basin of attraction of some stable configuration C_i ($i = 1, 2, \ldots, \mathcal{N}$). Taking a uniform grid parametrized by 'balls' of size l, we define the family of fractal dimensions D_q:

$$D_q = \frac{1}{q-1} \lim_{l \to 0} \frac{\ln \sum_{i=1}^{\mathcal{N}} \nu^q(C_i)}{\ln l}. \tag{1}$$

As q is varied, different subsets of ν^q associated with different values of q become dominant.

Let us define the scaling exponent α as follows:

$$\nu^q(C_i) \sim l^{\alpha q}$$

where α can take different values, corresponding to different regions of the measure which become dominant in equation (1). In particular, it is natural to suggest that $\sum_{i=1}^{\mathcal{N}} \nu^q(C_i)$ can be rewritten as follows:

$$\sum_{i=1}^{\mathcal{N}} \nu^q(C_i) = \left[\int \mathrm{d}\alpha' \, \rho(\alpha') l^{-f(\alpha')} l^{\alpha' q} \right]\Bigg|_{l \to 0}$$

where $\rho(\alpha)$ is the probability to have the value α lying in a small 'window' $[\alpha', \alpha' + \Delta\alpha']$ and $f(\alpha)$ is a continuous function which has the sense of a fractal dimension of the subset characterized by the value α.

Supposing $\rho(\alpha) > 0$, one can evaluate the last expression approximately via the saddle-point method. Thus, one obtains (see, for example, [1])

$$\frac{\mathrm{d}}{\mathrm{d}\alpha} f(\alpha) = q$$

$$\frac{\mathrm{d}^2}{\mathrm{d}\alpha^2} f(\alpha) < 0$$

which together with (1) leads to the following equations:

$$\begin{aligned} \tau(q) &= q\alpha(q) - f[\alpha(q)] \\ \alpha(q) &= \frac{\mathrm{d}}{\mathrm{d}q} \tau(q) \end{aligned} \tag{2}$$

where $\tau(q) = (q-1)D_q$. Hence, the exponents $\tau(q)$ and $f[\alpha(q)]$ are related via the Legendre transform. For further details and a more advanced mathematical analysis, the reader is referred to [9].

2.1. 2D topological systems and their relation to hyperbolic geometry

Topological constraints essentially modify physical properties of the broad class of statistical systems composed of chain-like objects. It should be stressed that topological problems are widely investigated in connection with quantum field and string theories, 2D gravitation, statistics of vortices in superconductors, the quantum Hall effect, thermodynamic properties of entangled polymers, etc. Modern methods of theoretical physics allow us to describe rather comprehensively the effects of non-Abelian statistics on the physical behaviour of some systems. However, the following question still remains obscure: what are the fractal (and as it is shown below, multifractal) properties of the distribution function of topological invariants, characterizing the homotopy states of a statistical system with topological constraints? We investigate this problem within the framework of the 'random walk in an array of obstacles' (RWAO) model.

The RWAO model can be regarded as physically clear and as a very representative image for systems of fluctuating chain-like objects with a full range of non-Abelian topological properties. This model is formulated as follows: suppose that a random walk of N steps of length a takes place on a plane between obstacles which form a simple 2D rectangular lattice with unit cell of size $c_x \times c_y$. We assume that the random walk cannot cross ('pass through') any obstacles.

It is convenient to begin with the lattice realization of the RWAO model. In this case the random path can be represented as an N-step random walk in a square lattice of size $a \times a$ ($a \leqslant c_y \leqslant c_x$)—see figure 1.

It had been shown previously (see, for example [10, 11]) that for $a = c_x = c_y$ a lattice random walk in the presence of a regular array of obstacles (punctures) on the dual lattice $\mathbb{Z}^2$ is topologically equivalent to a free random walk on a graph—a Cayley tree with branching number $z = 4$ (see figure 2). An outline of the derivation of this result is as follows. The different topological states of our model coincide with the elements of the homotopy group

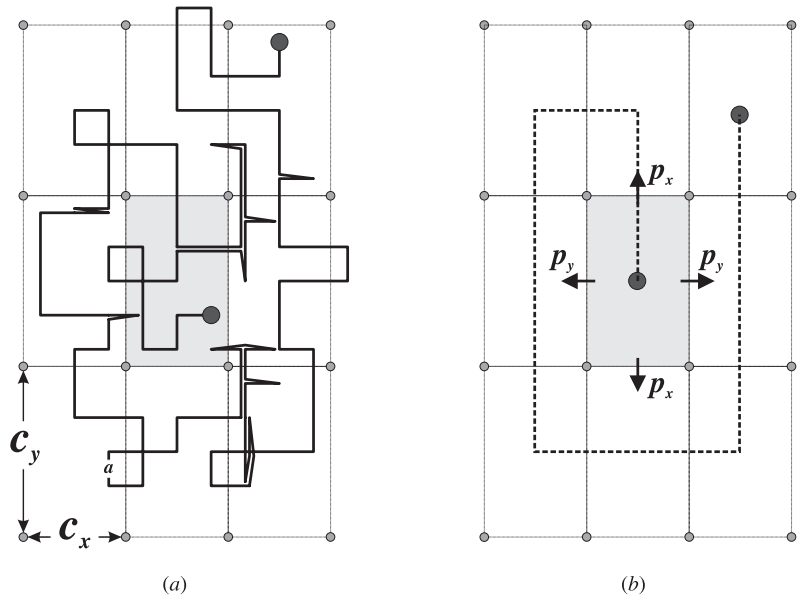

Figure 1. Random walk in the two-dimensional rectangular lattice of obstacles.

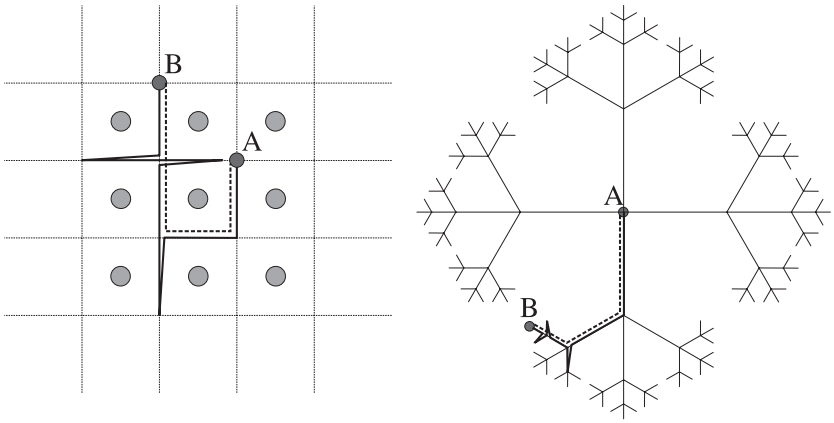

Figure 2. Random path for $a = c_x = c_y$: (*a*) in the 2D lattice of obstacles; (*b*) in the covering space (on the Cayley tree).

of the multi-punctured plane, which is the free group Γ_∞ generated by a countable set of elements. The translational invariance allows us to consider a local basis and therefore to study the factored group $\Gamma_\infty/\mathbb{Z}^2 = \Gamma_{z/2}$, where $\Gamma_{z/2}$ is a free group with $z/2$ generators whose Cayley graph is precisely a z-branching tree.

The relation between Cayley trees and hyperbolic geometry is discussed in detail in section 3. Intuitively, such a relation could be understood as follows. The Cayley tree can be isometrically embedded in the hyperbolic plane $\mathcal{H}$ (the surface of constant negative curvature). The group $\Gamma_{z/2}$ is one of the discrete subgroups of the group of motion of the hyperbolic plane $\mathcal{H} = SL(2,\mathbb{R})/SO(2)$, therefore the Cayley tree can be considered as a particular discrete realization of the hyperbolic plane.

Returning to the RWAO model, we conclude that each trajectory in the lattice of obstacles can be lifted to a path in the 'universal covering space', i.e to a path on the z-branching Cayley tree. The geodesic on the Cayley graph, i.e the shortest trajectory along the graph which connects ends of the path, plays the role of a complete topological invariant for the original trajectory in the lattice of obstacles. For example, the random walk in the lattice of obstacles is closed and contractible to a point (i.e. is not entangled with the array of obstacles) if and only if the geodesic length between the ends of the trajectory on the Cayley graph is zero. Hence, this geodesic length can be regarded as a topological invariant, which preserves the main non-Abelian features of the considered problem.

We would like to stress two facts concerning our model. (a) The exact configuration of a geodesic is a complete topological invariant, while its length k is only a partial topological invariant (except the case $k = 0$). (b) Geodesics have a clear geometrical interpretation, having the sense of a bar (or 'primitive') path which remains after deleting all even-times folded parts of a random trajectory in the lattice of obstacles. The concept of 'primitive path' has been used repeatedly in the statistical physics of polymers, leading to a successful classification of the topological states of chain-like molecules in various topological problems [10–12].

Even if many aspects of the statistics of random walks in fixed lattices of obstacles have been well understood (see, for example, [13] and references therein), the set of problems dealing with the investigation of fractal properties of the distribution of topological invariants in the RWAO model are practically out of discussion. Thus we devote the next section to the

study of fractal and multifractal structures of the measure on the set of primitive paths in the RWAO model for $a \ll c_y < c_x$.

2.2. Multifractality of the measure on the set of primitive paths on a non-symmetric Cayley tree

The classification of different topological states of an N-step random walk in a rectangular lattice of obstacles in the case $a \ll c_y < c_x$ turns out to be a more difficult and richer problem than in the case $a = c_y = c_x$ discussed above. However, after a proper rescaling, the mapping of a random walk in the rectangular array of obstacles to a random walk on a Cayley tree can be explored again. To proceed we should solve two auxiliary problems. First of all we consider a random walk inside the elementary rectangular cell of the lattice of obstacles. Let us compute:

(a) the 'waiting time', i.e the average number of steps $\langle t \rangle$ which a t-step random walk spends within a rectangle of size $c_x \times c_y$;
(b) the ratio of the 'escape probabilities' p_x and p_y through the corresponding sides c_x and c_y for a random walk staying until time t within the elementary cell.

The desired quantities can be easily computed from the distribution function $P(x_0, y_0, x, y, t)$ which gives the probability of finding the t-step random walk with initial (x_0, y_0) and final (x, y) points within the rectangle of size $c_x \times c_y$. The function $P(x, y, t)$ in the continuous approximation ($a \to 0$; $t \to \infty$; $at =$ constant) is the solution of the following boundary problem:

$$\begin{aligned} &\frac{\partial}{\partial t} P(x, y, t) = \tfrac{1}{4} a^2 \left(\frac{\partial^2}{\partial x^2} + \frac{\partial^2}{\partial y^2} \right) P(x, y, t) \\ &P(0, y, t) = P(c_x, y, t) = P(x, 0, t) = P(x, c_y, t) = 0 \\ &P(x, y, 0) = \delta(x_0, y_0) \end{aligned} \tag{3}$$

where a is the length of the effective step of the random walk and the value $\frac{1}{4}a^2$ has the sense of a diffusion constant.

The solution of equations (3) reads

$$\begin{aligned} P(x_0, y_0, x, y, t) = \frac{4}{c_x c_y} \sum_{m_x=1}^{\infty} \sum_{m_y=1}^{\infty} \exp\left\{ -\frac{\pi^2 a^2}{4} \left(\frac{m_x^2}{c_x^2} + \frac{m_y^2}{c_y^2} \right) t \right\} \\ \times \sin \frac{\pi m_x x_0}{c_x} \sin \frac{\pi m_y y_0}{c_y} \sin \frac{\pi m_x x}{c_x} \sin \frac{\pi m_y y}{c_y}. \end{aligned} \tag{4}$$

The 'waiting time' $\langle t \rangle$ can now be written as follows:

$$\langle t \rangle = \frac{1}{c_x c_y} \int_0^{c_x} \mathrm{d}x_0 \int_0^{c_y} \mathrm{d}y_0 \int_0^{c_x} \mathrm{d}x \int_0^{c_y} \mathrm{d}y \int_0^{\infty} \mathrm{d}t \; P(x_0, y_0, x, y, t) \tag{5}$$

while the ratio p_x/p_y can be computed straightforwardly via the relation

$$\frac{p_x}{p_y} = \frac{\int_0^{c_x} \mathrm{d}x_0 \int_0^{c_y} \mathrm{d}y_0 \int_0^{c_x} \mathrm{d}x \; P(x_0, y_0, x, y, t)\big|_{y=\{a, c_y - a\}}}{\int_0^{c_x} \mathrm{d}x_0 \int_0^{c_y} \mathrm{d}y_0 \int_0^{c_y} \mathrm{d}y \; P(x_0, y_0, x, y, t)\big|_{x=\{a, c_x - a\}}}. \tag{6}$$

In the 'ground state dominance' approximation we truncate the sum (4) at $m_x = m_y = 1$ and obtain the following approximate expressions:

$$\langle t \rangle = \frac{4^4 \, c_x^2 \, c_y^2}{\pi^6 \, a^2 \, (c_x^2 + c_y^2)} \qquad \frac{p_x}{p_y} = \frac{c_x^2}{c_y^2}. \tag{7}$$

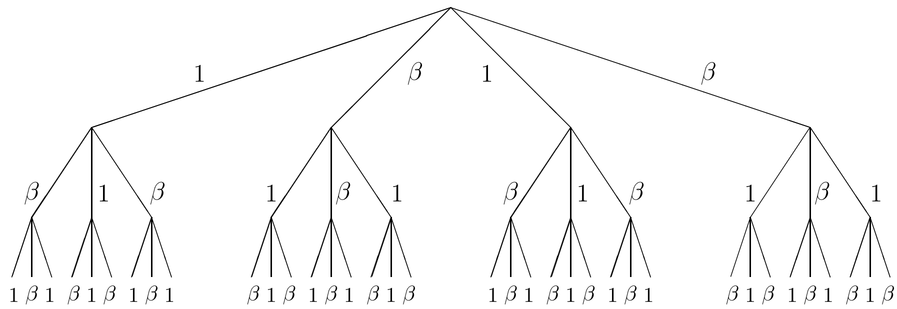

Figure 3. Four-branching Cayley tree with different transition probabilities along branches.

In the symmetric case ($c_x = c_y \equiv c$) equation (7) gives $\langle t\rangle = 2^7\, c^2/\pi^6\, a^2$ and $p_x/p_y = 1$, as it should for a square lattice of obstacles.

Now the distribution function of the primitive paths for the RWAO model can be obtained via lifting this topological problem to the problem of *directed* random walks† on the four-branching Cayley tree, where the random walk on the Cayley tree is defined as follows.

(a) The total number of steps $\tilde{N}$ on the Cayley tree is

$$\tilde{N} = \frac{N}{\langle t\rangle} = \frac{\pi^6}{4^4}\,\frac{Na^2(c_x^2 + c_y^2)}{c_x^2\, c_y^2}$$

(the value $\langle t\rangle$ has been computed in (7)).

(b) The distance (or 'level' k) on the Cayley tree is defined as the number of steps of the shortest path between two points on the tree. Each vertex of the Cayley tree has four branches; the steps along two of them carry a Boltzmann weight of 1, while the steps along the two remaining ones carry a Boltzmann weight β as shown in figure 3. The value of β is fixed by equation (7), which yields

$$\beta = \frac{p_x}{p_y} = \frac{c_x^2}{c_y^2}. \tag{8}$$

The ultrametric structure of the topological phase space, i.e. of the Cayley tree $\gamma(\beta)$, allows us to use the results of paper [1] to investigate the multicritical properties of the measure of all primitive (directed) paths of k steps along the graph $\gamma(\beta)$ with non-symmetric weights 1 and β (see figure 3). A rigorous mathematical description of such weighted paths on trees (called cascades) can be found in [25], where the authors derive multifractal spectra, but for different distributions of weights.

We construct the partition function $\Omega(\beta, k)$ which counts properly the weighted number of all $4 \times 3^{k-1}$ different k-step primitive paths on the graph $\gamma(\beta)$.

Define two partition functions a_k and b_k of k-step paths, whose last steps carry the weights 1 and β correspondingly. These functions satisfy the recursion relations for $k \geqslant 1$:

$$\begin{aligned} a_{k+1} &= a_k + 2\, b_k \\ b_{k+1} &= 2\beta\, a_k + \beta\, b_k \end{aligned} \qquad (k \geqslant 1) \tag{9}$$

† Recall that by definition the primitive path is the geodesic distance and therefore cannot have two successive opposite steps.

with the following initial conditions at $k = 1$:

$$\begin{aligned} a_1 &= 2 \\ b_1 &= 2\beta. \end{aligned} \tag{10}$$

Combining (9) and (10) we arrive at the following two-step recursion relation for the function a_k:

$$\begin{aligned} a_{k+2} &= (1+\beta)\, a_{k+1} + 3\beta\, a_k \qquad && (k \geqslant 1) \\ a_1 &= 2 && (k = 1) \\ a_2 &= 2 + 4\beta && (k = 2) \end{aligned} \tag{11}$$

whose solution is

$$a_k = \frac{a_2 - a_1\lambda_2}{\lambda_1 - \lambda_2}\lambda_1^{k-1} + \frac{a_1\lambda_1 - a_2}{\lambda_1 - \lambda_2}\lambda_2^{k-1} \tag{12}$$

where

$$\lambda_{1,2} = \tfrac{1}{2}\Big(1 + \beta \pm \sqrt{(1+\beta)^2 + 12\beta}\Big). \tag{13}$$

Taking into account that b_k is given by the same recursion relation as a_k, but with the initial values $b_1 = 2\beta$ and $b_2 = 2\beta^2 + 4\beta$, we obtain the following expression for the partition function $\Omega(\beta, k) = a_k + b_k$:

$$\Omega(\beta, k) = \frac{2(1 + 4\beta + \beta^2) - 2(1+\beta)\lambda_2}{\lambda_1 - \lambda_2}\lambda_1^{k-1} + \frac{2(1+\beta)\lambda_1 - 2(1 + 4\beta + \beta^2)}{\lambda_1 - \lambda_2}\lambda_2^{k-1}. \tag{14}$$

The partition function $\Omega(\beta, k)$ contains all necessary information about the multifractal behaviour. Following equations (1) and (2), we associate the set of stable configurations $\{C_i\}$ with the set of $\mathcal{N}(k) = 4 \times 3^{k-1}$ vertices of level k. Hence, we define

$$\sum_{i=1}^{\mathcal{N}} \nu^q(C_i) = \frac{\Omega(\beta^q, k)}{\Omega^q(\beta, k)}. \tag{15}$$

Taking into account that the uniform grid has resolution $l(k) = 1/\mathcal{N}(k)$ for $k \geqslant 1$ and using equation (1), we obtain

$$\tau(q) = \lim_{k\to\infty} \frac{\ln \Omega(\beta^q, k) - q \ln \Omega(\beta, k)}{\ln l(k)} \tag{16}$$

which allows us to determine the generalized Hausdorff dimension D_q via the relation

$$D_q = \tau(q)/(q-1). \tag{17}$$

The corresponding plots of the functions $D_q(q)$ for different values of $\beta = \{0.001;\ 0.01;\ 0.1;\ 0.5\}$ are shown in figure 4 (the numerical computations of equations (16) and (17) are carried out for $k = 100\,000$). The fact that $D_q(q)$ depends on q clearly demonstrates the multifractal behaviour.

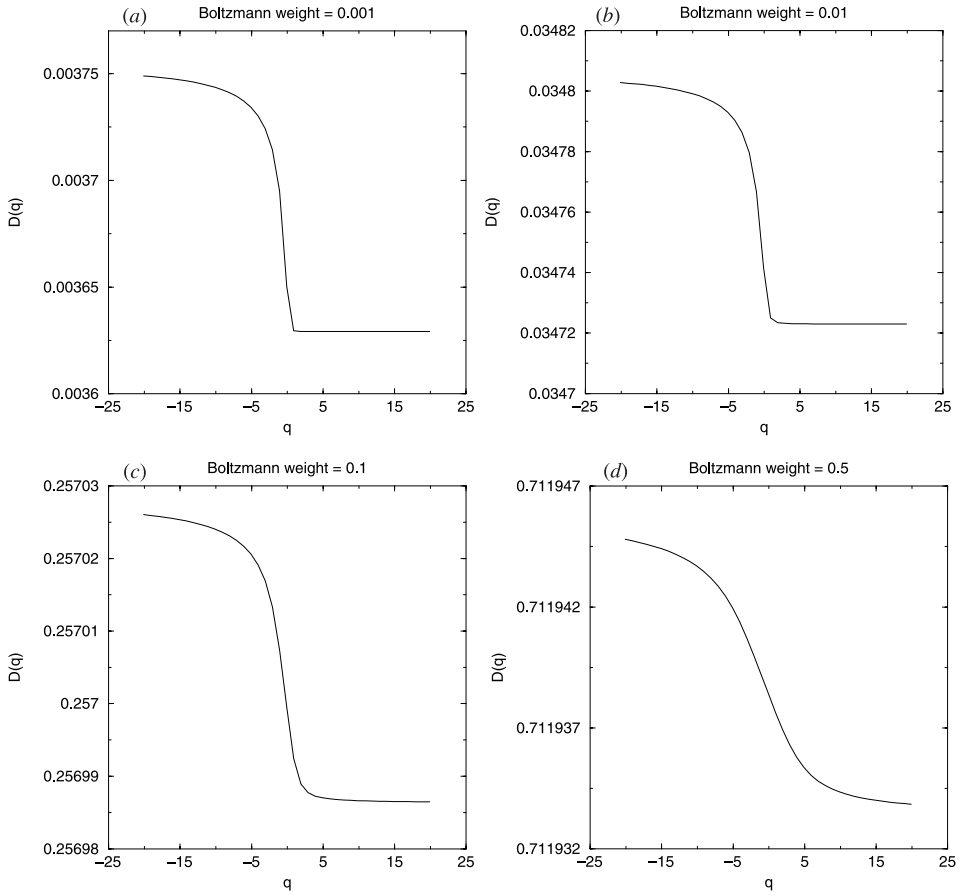

Figure 4. Dependence $D_q(q)$ for different values of Boltzmann weight β.

3. Random walk on a non-symmetric Cayley tree

3.1. Master equation

Consider a random walk on a four-branching Cayley tree and investigate the distribution $P(k, \tilde{N})$ giving the probability for an $\tilde{N}$-step random walk starting at the origin of the tree to have a primitive (shortest) path between ends of length k. The random walk is defined as follows: at each vertex of the Cayley tree the probability of a step along two of the branches is p_x, and is p_y along the two others; p_x and p_y satisfy the conservation condition $2p_x + 2p_y = 1$. Using equation (8), the following expressions hold:

$$\begin{aligned} p_x &= \frac{\beta}{2(1+\beta)} \\ p_y &= \frac{1}{2(1+\beta)}. \end{aligned} \tag{18}$$

The symmetric case $\beta = 1$ (which gives $p_x = p_y = \frac{1}{4}$) has already been studied and an exact expression for $P(k, \tilde{N})$ has been derived in [14]. A rigorous mathematical description of random walks on graphs can be found in [16]. The importance of spherical symmetry (i.e.

the fact that all vertices of a given level are strictly equivalent) is discussed in [23]. Another example of a non-symmetric model on a tree (the case of randomly distributed transition probabilities, the so-called RWRE model) is described in [24]. To the best of our knowledge, the solution for the non-symmetric random walk which we defined above is known only for k fixed and $\tilde{N} \gg 1$ [15]. Here we consider the case $k \gg 1$, $\tilde{N} \gg 1$, and, in particular, we study the distribution in the neighbourhood of the maximum. Breaking the symmetry by taking $\beta \neq 1$ strongly affects the structure of the problem, since then the phase space becomes locally non-uniform. We now have vertices of two different kinds, x and y, depending on whether the step toward the root of the Cayley tree occurs with probability p_x or p_y. In order to obtain a master equation for $P(k, \tilde{N})$, we introduce the new variables $L_x(k, \tilde{N})$ and $L_y(k, \tilde{N})$, which define the probabilities to be at level k in a vertex x or y after $\tilde{N}$ steps. In the same way we recursively define the probabilities $L_{a_1 \dots a_n}(k, \tilde{N})$, $(a_i = \{x, y\})$ to be at level k in a vertex such that the sequence of vertices toward the root of the tree is $a_1 \dots a_n$. One can see that the recursion depends on the total 'history' up to the root point, which makes the problem non-local. The master equation for the distribution function $P(k, \tilde{N})$,

$$P(k, \tilde{N}+1) = (2p_x + p_y)L_y(k-1, \tilde{N}) + (2p_y + p_x)L_x(k-1, \tilde{N}) + p_y L_y(k+1, \tilde{N}) + p_x L_x(k+1, \tilde{N}) \tag{19}$$

is coupled to the hierarchical set of functions $\{L_x, L_y; L_{xx}, L_{xy}, L_{yx}, L_{yy}; \dots; L_{a_1 \dots a_n}\}$ which satisfy the following recursion relation:

$$L_{a_1 \dots a_n}(k, \tilde{N}+1) = (2 - \delta_{a_1, a_2}) p_{a_1} L_{a_2 \dots a_n}(k-1, \tilde{N}) + p_x L_{x a_1 \dots a_n}(k+1, \tilde{N}) + p_y L_{y a_1 \dots a_n}(k+1, \tilde{N}) \tag{20}$$

where $a_1 \dots a_n$ cover all sequences of any lengths $(\leqslant k)$ in x and y. In order to close this infinite system at an arbitrary order n_0 we make the following assumption: for any $n \leqslant n_0$ we have

$$\left. \frac{L_{a_1 \dots a_n}(k, \tilde{N})}{P(k, \tilde{N})} \right|_{\substack{k \gg n_0 \\ \tilde{N} \gg n_0}} \longrightarrow \alpha_{a_1 \dots a_n} \tag{21}$$

with $\alpha_{a_1 \dots a_n}$ constant.

Using the approximation (21) we rewrite (19)–(20) for large k and $\tilde{N}$ in terms of the function $P(k, \tilde{N})$ and constants $\alpha_{a_1 \dots a_n}$ $(0 < n \leqslant n_0)$. Taking into account that

$$L_{a_1 \dots a_n x} + L_{a_1 \dots a_n y} = L_{a_1 \dots a_n}$$

we arrive at $2^{n_0 - 1}$ independent recursion relations for one and the same function $P(k, \tilde{N})$, with $2^{n_0} - 1$ independent unknown constants $\alpha_{a_1 \dots a_{n_0}}$. In order to make this system self-consistent, one has to identify coefficients entering in different equations, which yields $2^{n_0} - 2$ compatibility relations for the constants $\alpha_{a_1 \dots a_{n_0}}$, and the system is still open. This fact means that all scales are involved and the evolution of $L_{a_1 \dots a_n}$ depends on $L_{a_1 \dots a_{n+1}}$, the evolution of $L_{a_1 \dots a_{n+1}}$ depends on $L_{a_1 \dots a_{n+2}}$ and so on. At each scale we need information about larger scales. This kind of scaling problem naturally suggests the use of a renormalization-group approach, which is developed in the next section.

To begin the renormalization procedure, we need to estimate the values of the constants $\alpha_{a_1 \dots a_{n_0}}$ for the first (i.e. the smallest) scale. Let us denote

$$\alpha_x = \alpha$$

$$\alpha_y = 1 - \alpha$$

and define $\alpha_{xx}, \alpha_{xy}, \alpha_{yy}, \alpha_{yx}$ as follows:

$$\begin{aligned}\alpha_{xx} &= v_x\alpha\\ \alpha_{yy} &= v_y(1-\alpha)\\ \alpha_{xy} &= (1-v_x)\alpha\\ \alpha_{yx} &= (1-v_y)(1-\alpha).\end{aligned}$$

Now we set

$$p_x\alpha_{xa_1\ldots a_n} + p_y\alpha_{ya_1\ldots a_n} = \big(p_x\alpha + p_y(1-\alpha)\big)\alpha_{a_1\ldots a_n} \tag{22}$$

which means that we neglect the correlations between the constants $\alpha_{a_1\ldots a_n}$ and $\alpha_{a_2\ldots a_n}$ at different scales. As is shown in the next section, the renormalization-group approach allows us to get rid of the approximation (22).

With (22) one can obtain the following generic master equation:

$$P(k,\tilde{N}+1) = \frac{p_{a_1}\alpha_{a_2\ldots a_n}}{\alpha_{a_1\ldots a_n}}(2-\delta_{a_1,a_2})P(k-1,\tilde{N}) + \big(\alpha p_x + (1-\alpha)p_y\big)P(k+1,\tilde{N}) \tag{23}$$

where $a_1\ldots a_n$ again cover all possible sequences in x and y. We have now $2^{n_0}-1$ unknown quantities with $2^{n_0}-1$ compatibility relations (23), which makes the system (23) closed.

For illustration, we derive the solution for $n_0 = 2$:

$$\begin{aligned}P(k,\tilde{N}+1) &= \frac{p_x}{v_x}P(k-1,\tilde{N}) + \big(\alpha p_x + (1-\alpha)p_y\big)P(k+1,\tilde{N})\\ P(k,\tilde{N}+1) &= \frac{2p_x(1-\alpha)}{\alpha(1-v_x)}P(k-1,\tilde{N}) + \big(\alpha p_x + (1-\alpha)p_y\big)P(k+1,\tilde{N})\\ P(k,\tilde{N}+1) &= \frac{p_y}{v_y}P(k-1,\tilde{N}) + \big(\alpha p_x + (1-\alpha)p_y\big)P(k+1,\tilde{N})\\ P(k,\tilde{N}+1) &= \frac{2p_y\alpha}{(1-\alpha)(1-v_y)}P(k-1,\tilde{N}) + \big(\alpha p_x + (1-\alpha)p_y\big)P(k+1,\tilde{N}).\end{aligned} \tag{24}$$

Note that (24) clearly displays a $\mathbb{Z}_2$ symmetry: $p_x \to p_y,\ \alpha \to -\alpha,\ v_x \to v_y$. Compatibility conditions for the system (24) read

$$\frac{p_x}{v_x} = \frac{p_y}{v_y} = \frac{2p_x(1-\alpha)}{\alpha(1-v_x)} = \frac{2p_y\alpha}{(1-\alpha)(1-v_y)} \tag{25}$$

which finally gives

$$\begin{aligned}\alpha &= \frac{-1-3\beta+\sqrt{1+14\beta+\beta^2}}{2(1-\beta)}\\ v_x &= \frac{\alpha}{2-\alpha}\\ v_y &= \frac{1-\alpha}{1+\alpha}.\end{aligned} \tag{26}$$

As has been said above, without (22) the system (19) and (20) is open, giving a single equation for the unknown function $P(k,\tilde{N})$ depending on the unknown parameter α:

$$\begin{aligned}P(k,\tilde{N}+1) = &\big((2p_x+p_y)(1-\alpha) + (2p_y+p_x)\alpha\big)P(k-1,\tilde{N})\\ &+\big(p_y(1-\alpha)+p_x\alpha\big)P(k+1,\tilde{N}).\end{aligned} \tag{27}$$

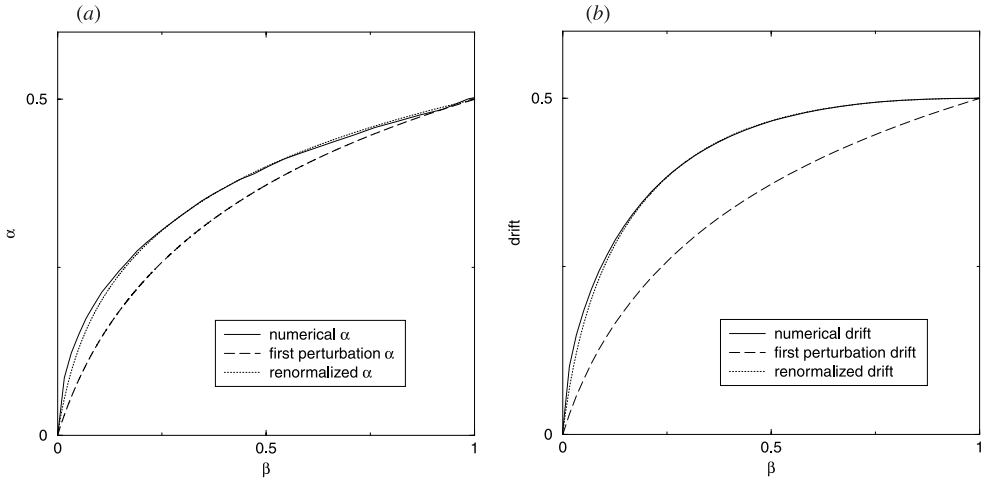

Figure 5. The values of α and $\bar{k}$ compared with renormalized quantities and numerical simulations: (*a*) vortex-type distribution; (*b*) drift.

Equation (27) describes a 1D diffusion process with a drift

$$\frac{\langle k\rangle}{\tilde{N}} \equiv \bar{k} = 2\alpha p_y + 2(1-\alpha)p_x \tag{28}$$

and a dispersion

$$\delta = \frac{\langle k - \langle k\rangle\rangle^2}{\tilde{N}} = 1 - 4\big(\alpha p_y + (1-\alpha)p_x\big)^2 \tag{29}$$

which provides for $k \gg 1$ and $\tilde{N} \gg 1$ the usual Gaussian distribution with non-zero mean (see [10]). The value of α obtained in (26) using the approximation (22) gives a fair estimate of the drift compared with the numerical simulations, as is shown in figure 5.

3.2. Real space renormalization

In order to improve the results obtained above, we recover the information lost in the approximation (22) and take into account 'interactions' between different scales. Namely, we follow the renormalization flow of the parameter $\alpha(l)$ at a scale l, supposing that a new effective step is a composition of 2^l initial lattice steps. Let us define:

- the probability $f_a(l)$ of going forth (with respect to the location of the root point of the Cayley tree) from a vertex of kind a;
- the probability $b_a(l)$ of going back (towards the root point of the Cayley tree) from a vertex of kind a;
- the probability $\alpha(l)$ of being at a vertex of kind x;
- the conditional probability $w_a(l)$ to reach a vertex of kind a starting from a vertex of kind a under the condition that the step is forth;
- the conditional probability $v_a(l)$ to reach a vertex of kind a starting from a vertex of kind a under the condition that the step is back;
- the effective length $d(l)$ of a composite step.

Then the drift $\overline{k}(l)$ at scale l is given by (compare with (28))

$$\overline{k}(l) = d(l)\left[\alpha(l)\big(f_x(l) - b_x(l)\big) + \big(1-\alpha(l)\big)\big(f_y(l) - b_y(l)\big)\right]. \tag{30}$$

We say that the problem is scale-independent if the flow $\overline{k}(l)$ is invariant under the decimation procedure, i.e. with respect to the renormalization group. We compute the flow counting the appropriate combinations of two steps, depending on the variable considered:

$$\begin{aligned}
w_a(l+1) &= \big(1-w_a(l)\big)\big(1-w_{\bar a}(l)\big) + w_a^2(l)\\
v_a(l+1) &= \big(1-v_a(l)\big)\big(1-v_{\bar a}(l)\big) + v_a^2(l)\\
f_a(l+1) &= \frac{f_a(l)\left[w_a(l)f_a(l) + \big(1-w_a(l)\big)f_{\bar a}(l)\right]}{c_a(l)}\\
b_a(l+1) &= \frac{b_a(l)\left[v_a(l)b_a(l) + \big(1-v_a(l)\big)b_{\bar a}(l)\right]}{c_a(l)}\\
d(l+1) &= d(l)\left[\alpha(l)c_x(l) + \big(1-\alpha(l)\big)c_y(l)\right]\\
\alpha(l+1) &= \overline{k}(l)\left[\alpha(l)w_x(l) + \big(1-\alpha(l)\big)\big(1-w_y(l)\big)\right]\\
&\quad + \big(1-\overline{k}(l)\big)\left[\alpha(l)v_x(l) + \big(1-\alpha(l)\big)\big(1-v_y(l)\big)\right]
\end{aligned} \tag{31}$$

where $\bar a = x$ when $a = y$ (and $\bar a = y$ when $a = x$) and the value $c_a(l)$ ensures the conservation condition $f_a(l+1)+b_a(l+1) = 1$ because we do not consider the combinations of two successive steps in opposite directions.

The transformation of α in (31) needs some explanation. We consider the drift $\overline{k}(l)$ as a probability to make a (composite) step forward. The equation for α is given by counting the different ways of getting to a vertex of kind x. One can check that $\overline{k}(l)$ given by (30) remains invariant under such a transformation, which is considered as a verification of the scale independence (i.e. of renormalizability).

Following the standard procedure, we find the fixed points for the flow of $\alpha(l)$. First of all we realize that the recursion equations for $w_a(l)$ and $v_a(l)$ can be solved independently, providing a continuous set of fixed points: $w_x^0 = 1 - w_y^0$ and $v_x^0 = 1 - v_y^0$. Using the initial conditions (26) for $v_a(l)$ and deriving straightforwardly the absent initial conditions for $w_a(l)$, we obtain

$$\begin{aligned}
v_x(1) &= v_x\\
v_y(1) &= v_y\\
w_x(1) &= w_x = \frac{p_x}{p_x + 2p_y}\\
w_y(1) &= w_y = \frac{p_y}{p_y + 2p_x}
\end{aligned} \tag{32}$$

(we recall that these values are obtained by taking into account the elementary correlations for two successive steps).

With the initial conditions (32) we find the following renormalized values v^0 and w^0 at the fixed point:

$$\begin{aligned}
v^0 = v^0(\beta) &= \lim_{l\to\infty} v_x(l) = 1 - \lim_{l\to\infty} v_y(l) = \tfrac{1}{2}\left[(v_x - v_y)\prod_{n=1}^{\infty} f^{(n)}(v_x + v_y) + 1\right]\\
w^0 = w^0(\beta) &= \lim_{l\to\infty} w_x(l) = 1 - \lim_{l\to\infty} w_y(l) = \tfrac{1}{2}\left[(w_x - w_y)\prod_{n=1}^{\infty} f^{(n)}(w_x + w_y) + 1\right]
\end{aligned} \tag{33}$$

where $f^{(n)}(x)$ is the nth iteration of the function

$$f(x) = x^2 - 2x + 2.$$

We then obtain successively all renormalized values at the fixed point

$$\begin{aligned} f_a^0 &= 1 \\ b_a^0 &= 0 \\ d^0 = \overline{k^0} &= \frac{\alpha^0 + \beta(1-\alpha^0)}{1+\beta} \\ \alpha^0 &= \frac{v^0 + \beta w^0}{1+\beta+(1-\beta)(v^0 - w^0)} \end{aligned} \tag{34}$$

where the invariance of the drift $\overline{k}$ is taken into account:

$$\overline{k^0} = \overline{k}(1) = 2p_y\alpha^0 + 2p_x(1-\alpha^0) = \frac{\alpha^0 + \beta(1-\alpha^0)}{1+\beta}.$$

In figure 5 we compare the theoretical results with numerical simulations. It is worth mentioning the efficiency of the renormalization-group method, which yields a solution in very good agreement with numerical simulations in a broad interval of values β.

In addition, we compare our results with the exact expression obtained by Gerl and Woess in [15] for the probability $P(0, \tilde{N})$ to return to the origin after $\tilde{N}$ random steps on the non-symmetric Cayley tree. This distribution function $P(0, \tilde{N})$ reads

$$P(0, \tilde{N}) \propto \mu^{\tilde{N}}\, \tilde{N}^{-3/2} \tag{35}$$

with

$$\mu \equiv \mu(\beta) = \min\left\{-t + \sqrt{t^2 + 4p_x^2} + \sqrt{t^2 + 4p_y^2}\ \middle|\ t > 0\right\}. \tag{36}$$

Let us now assert, without justification, that equation (27) (which is actually written for $k \gg 1$ and $\tilde{N} \gg 1$) is valid for any values of k and $\tilde{N}$. The initial conditions for the recursion relation (27) are as follows:

$$\begin{aligned} P(0, \tilde{N}+1) &= \big(2\alpha p_x + 2(1-\alpha)p_y\big) P(1, \tilde{N}) \\ P(k, 0) &= \delta_{k,0}. \end{aligned} \tag{37}$$

One can note that equation (27) completed with the conditions (37) can be viewed as a master equation for a *symmetric* random walk on a Cayley tree *with effective branching* z continuously dependent on β:

$$z(\beta) = \frac{2}{\alpha p_x + (1-\alpha)p_y}. \tag{38}$$

Hence, we conclude that our problem becomes equivalent to a symmetric random walk on a $z(\beta)$-branching tree. For $k = 0$ the solution, given in [10] is

$$P(0, \tilde{N}) \propto \left[\frac{2\sqrt{z(\beta)-1}}{z(\beta)}\right]^{\tilde{N}} \tilde{N}^{-3/2}. \tag{39}$$

This provides the same form as the exact solution (35). It has been checked numerically that for $\beta \in \mathbb{R}^+$ the discrepancy between (35) and (39) is as follows:

$$\frac{1}{\mu(\beta)}\left|\frac{2\sqrt{z(\beta)-1}}{z(\beta)} - \mu(\beta)\right| < 0.02.$$

Thus, we believe that our self-consistent RG approach to the statistics of random walks on non-symmetric trees can be extended with sufficient accuracy to all values of k.

4. Multifractality and the locally non-uniform curvature of Riemann surfaces

We have claimed in sections 1 and 2 that local non-uniformity and the exponentially growing structure of the phase space of statistical systems generate a multiscaling behaviour of the corresponding partition functions. The aim of the present section is to bring geometric arguments to support our claim by introducing a different approach to the RWAO model. The differences between the approach considered in this section and that discussed in section 2 are as follows:

- we consider a *continuous* model of a random walk topologically entangled with either a symmetric or a non-symmetric *triangular* lattice of obstacles on the plane;
- we pursue the goal to construct *explicitly* the metric structure of the topological phase space via conformal methods and *to relate directly the non-uniform fractal relief* of the topological phase space *to the multifractal properties* of the distribution function of topological invariants for the given model.

Consider a random walk in a regular array of topological obstacles on the plane. As in the discrete case we can split the distribution function of all N-step paths with fixed positions of end points into different topological (homotopy) classes. We characterize each topological class by a topological invariant similar to the 'primitive path' defined in section 2. Introducing complex coordinates $z = x + \mathrm{i}y$ on the plane, we use conformal methods which provide an efficient tool for investigating multifractal properties of the distribution function of random trajectories in homotopy classes.

Let us stress that explicit expressions are constructed so far for triangular lattices of obstacles only. That is why we replace the investigation of the rectangular lattices discussed in sections 1 and 2 by the consideration of the triangular ones. Moreover, for triangular lattices a continuous symmetry parameter (such as $\beta = c_x^2/c_y^2$ in the case of rectangular lattices) does not exist and only the triangles with angles $(\pi/3, \pi/3, \pi/3)$, $(\pi/2, \pi/4, \pi/4)$, $(\pi/2, \pi/6, \pi/3)$ are available—only such triangles tessellate the whole plane z. In spite of the mentioned restrictions, the study of these cases enables us to figure out the origin of multifractality coming from the metric structure of the topological phase space.

Suppose that the topological obstacles form a periodic lattice in the z-plane. Let the fundamental domain of this lattice be the triangle ABC with angles either $(\pi/3, \pi/3, \pi/3)$ (symmetric case) or $(\pi/2, \pi/6, \pi/3)$ (non-symmetric case). The conformal mapping $z(\zeta)$ establishes a one-to-one correspondence between a given fundamental domain ABC of the lattice of obstacles in the z-plane with a zero-angled triangle $\mathcal{ABC}$ lying in the upper half-plane $\eta > 0$ of the plane $\zeta = \xi + \mathrm{i}\eta$, and having corners on the real axis $\eta = 0$. To avoid

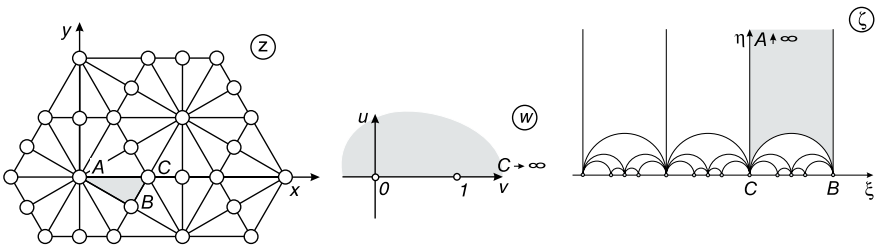

Figure 6. Conformal mapping of the complex plane z to the 'lacunary' upper half-plane $\mathrm{Im}\,\zeta > 0$ endowed with a Poincaré metric. The zero-angled triangle $\mathcal{ABC}$ on ζ corresponds to the triangle ABC with the angles $(\pi/2, \pi/6, \pi/3)$ on z.

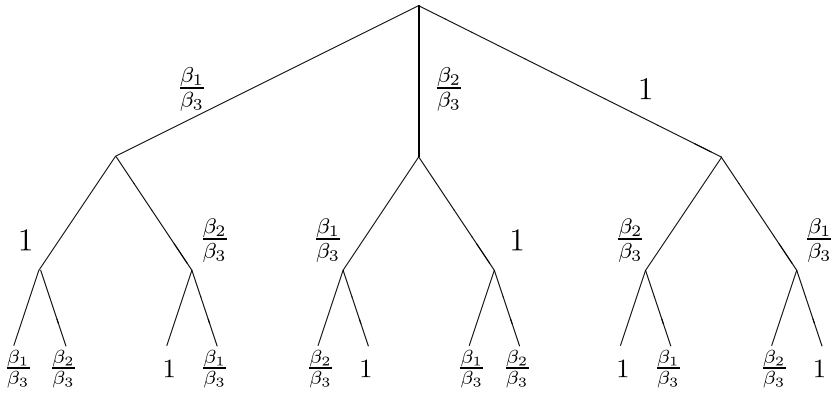

Figure 7. Non-symmetric three-branching Cayley tree.

possible misunderstandings let us point out that such a transform is conformal everywhere except at corner (branching) points (see, for example, [17]). Now consider the tessellation of the z-plane by means of consecutive reflections of the domain ABC with respect to its sides, and the corresponding reflections (inversions) of the domain $\mathcal{ABC}$ in the ζ-plane. The first few generations are shown in figure 6. The obtained upper half-plane $\mathrm{Im}\,\zeta > 0$ has a 'lacunary' structure and represents the topological phase space of the trajectories entangled with the lattice of obstacles. The details of such a construction as well as a discussion of the topological features of the conformal mapping $z(\zeta)$ in the symmetric case can be found in [13]. We recall the basic properties of the transform $z(\zeta)$ related to our investigation of multifractality.

The topological state of a trajectory C in the lattice of obstacles can be characterized as follows.

- Perform the conformal mappings $z_{\mathrm{s}}(\zeta)$ (or $z_{\mathrm{ns}}(\zeta)$) of the plane z with a symmetric (or non-symmetric) triangular lattice of obstacles to the upper half-plane $\mathrm{Im}\,\zeta > 0$, playing the role of the topological phase space of the given model.
- Connect by nodes the centres of neighbouring curvilinear triangles in the upper half-plane $\mathrm{Im}\,\zeta > 0$ and raise a graph γ_{s} (or γ_{ns}) (which is, as shown below an isometric Cayley tree embedded in the Poincaré plane).
- Find the image of the path C in the 'covering space' $\mathrm{Im}\,\zeta > 0$ and define the shortest (primitive) path connecting the centres of the curvilinear triangles where the ends of the path C are located. The configuration of this primitive path projected to the Cayley tree γ_{s} (or γ_{ns}) plays the role of topological invariant for the model under consideration.

The Cayley trees $\gamma_{\mathrm{s,ns}}$ have the same topological content as that described in section 2, but here we determine the Boltzmann weights $\beta_1, \beta_2, \beta_3$ associated with passages between neighbouring vertices (see figure 7) directly from the metric properties of the topological phase space obtained via the conformal mappings $z_{\mathrm{s,ns}}(\zeta)$.

It is well known that random walks are conformally invariant; in other words, the diffusion equation on the plane z preserves its structure under a conformal transform, but the diffusion coefficient can become space-dependent [18]. Namely, under the conformal transform $z(\zeta)$ the Laplace operator $\Delta_z = \frac{\mathrm{d}^2}{\mathrm{d}z\,\mathrm{d}\overline{z}}$ is transformed in the following way:

$$\frac{\mathrm{d}^2}{\mathrm{d}z\,\mathrm{d}\overline{z}} = \frac{1}{|z'(\zeta)|^2}\frac{\mathrm{d}^2}{\mathrm{d}\zeta\,\mathrm{d}\overline{\zeta}}. \tag{40}$$

Before discussing the properties of the Jacobians $|z'(\zeta)|^2$ for the symmetric and non-symmetric transforms, it is more convenient to set up the following geometrical context. The connection between Cayley trees and surfaces of constant negative curvature has already been pointed out [13], mostly through volume growth considerations. Therefore, it becomes more natural to regard the upper half-plane $\mathrm{Im}\,\zeta > 0$ as the standard realization of the hyperbolic 2-space (surface of constant negative curvature R, with here arbitrarily $R = -2$), i.e. to consider the following metric:

$$\mathrm{d}s^2 = \frac{-2}{R\eta^2}(\mathrm{d}\xi^2 + \mathrm{d}\eta^2). \tag{41}$$

Let us rewrite the Laplace operator (40) in the form

$$\frac{\mathrm{d}^2}{\mathrm{d}z\,\mathrm{d}\bar{z}} = D(\xi,\eta)\,\eta^2\left(\frac{\mathrm{d}^2}{\mathrm{d}\xi^2} + \frac{\mathrm{d}^2}{\mathrm{d}\eta^2}\right) \tag{42}$$

where the value $D(\xi,\eta) \equiv D(\zeta)$ can be interpreted as the normalized space-dependent diffusion coefficient on the Poincaré upper half-plane:

$$D(\zeta) = \frac{1}{\eta^2\,|z'(\zeta)|^2}. \tag{43}$$

The methods providing the conformal transform $z_{\mathrm{s}}(\zeta)$ for the symmetric triangle with angles $(\pi/3, \pi/3, \pi/3)$ have been discussed in details in [17]. The generalization of these results to the conformal transform $z_{\mathrm{ns}}(\zeta)$ for the non-symmetric triangle with angles $(\pi/2, \pi/6, \pi/3)$ is very straightforward. We expose here the Jacobians of those conformal mappings without derivation:

$$\begin{aligned} |z'_{\mathrm{s}}(\zeta)|^2 &= \frac{1}{\pi^{2/3}B^2\left(\frac{1}{3},\frac{1}{3}\right)}\left|\theta'_1(0,\mathrm{e}^{\mathrm{i}\pi\zeta})\right|^{8/3} \\ |z'_{\mathrm{ns}}(\zeta)|^2 &= \frac{\pi^2}{B^2\left(\frac{1}{2},\frac{1}{3}\right)}\left|\theta_0(0,\mathrm{e}^{\mathrm{i}\pi\zeta})\right|^{8/3}\left|\theta_2(0,\mathrm{e}^{\mathrm{i}\pi\zeta})\right|^4\left|\theta_3(0,\mathrm{e}^{\mathrm{i}\pi\zeta})\right|^{4/3} \end{aligned} \tag{44}$$

where $\theta'_1(\chi|\cdots) = \frac{\mathrm{d}}{\mathrm{d}\chi}\theta_1(\chi|\cdots)$ and $\theta_i(0|\cdots)$ $(i = 0,\ldots,3)$ are the standard definitions of Jacobi elliptic functions [19].

Combining (43) and (44) we define the effective inverse diffusion coefficients in symmetric (D_{s}^{-1}) and in non-symmetric (D_{ns}^{-1}) cases:

$$\begin{aligned} D_{\mathrm{s}}^{-1}(\zeta) &= \eta^2\left|z'_{\mathrm{s}}(\zeta)\right|^2 \\ D_{\mathrm{ns}}^{-1}(\zeta) &= \eta^2\left|z'_{\mathrm{ns}}(\zeta)\right|^2. \end{aligned} \tag{45}$$

The corresponding 3D plots of the reliefs $D_{\mathrm{s}}^{-1}(\xi,\eta)$ and $D_{\mathrm{s}}^{-1}(\xi,\eta)$ are shown in figure 8.

The functions $D_{\mathrm{s}}^{-1}(\zeta)$ and $D_{\mathrm{ns}}^{-1}(\zeta)$ are considered as quantitative indicators of the topological structure of the phase spaces; in particular, a Cayley tree can be isometrically embedded in the surface $D_{\mathrm{s}}^{-1}(\zeta)$. It can be shown that the images of the centres of the triangles of the symmetric lattice in the z-plane correspond to the local maxima of the surface $D_{\mathrm{s}}^{-1}(\zeta)$ in the ζ-plane. We define the vertices of the embedded tree as those maxima. The links connecting neighbouring vertices are defined in the next paragraph.

Let us define the *horocycles* which correspond to repeating sequences of weights in figure 7 with minimal periods. There are only three such sequences: $\beta_1\beta_2\beta_1\beta_2\ldots$, $\beta_1\beta_3\beta_1\beta_3\ldots$ and $\beta_2\beta_3\beta_2\beta_3\ldots$. The horocycles are images (analytically known) of certain circles of the z-plane. They proved to be a convenient tool for a constructive description of the trajectories in the z-plane starting from the trajectories in the covering space ζ.

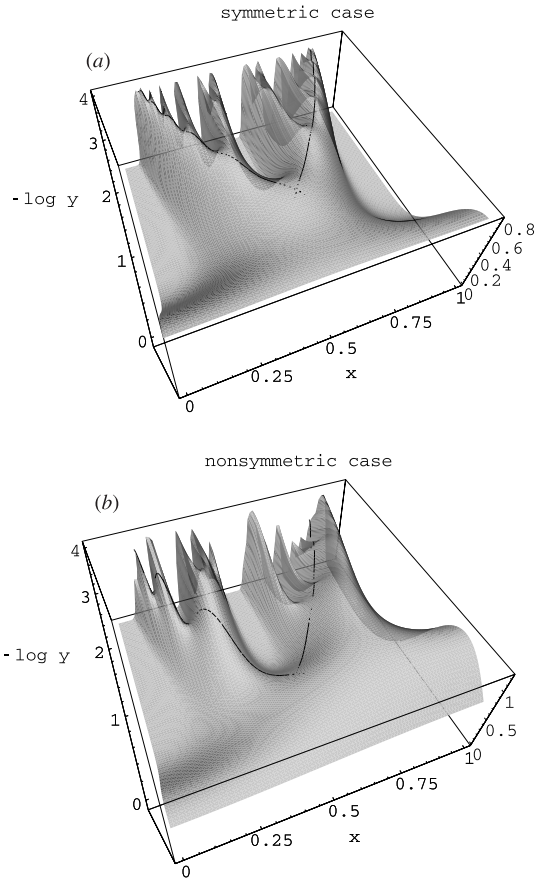

Figure 8. Profiles of the surfaces $D_{\rm s}^{-1}(\xi,\eta)$ and $D_{\rm ns}^{-1}(\xi,\eta)$ where $\xi \equiv x$, $\eta \equiv -\log y$. First generation of horocycles are shown by the lines.

The first generation of horocycles (closest to the root point of the Cayley tree) is shown in figure 8. Let us consider the symmetric case. Following a given horocycle we follow a ridge of the surface, and we pass through certain maxima of this surface (that is through certain vertices of the tree). We therefore define *locally* the links of the tree as the set of ridges connecting neighbouring maxima of $D_{\rm s}^{-1}(\xi,\eta)$. We recall that the ridge of the surface can be defined as the set of points where the gradient of the function $D_{\rm s}^{-1}(\xi,\eta)$ is minimal along its isoline. Even if this gives a proper definition of the tree, extracting a direct parametrization is difficult, that is why henceforth we will approximate the tree by arcs of horocycles.

To give a quantitative formulation of the local definition of the embedded Cayley tree, we consider the path integral formulation of the problem on the ζ-plane. Define the Lagrangian $\mathcal{L} \propto D_{\rm s}^{-1}(\zeta)\dot{\zeta}^2$ of a free particle moving with the diffusion coefficient $D_{\rm s}(\zeta)$ in the space ζ. Following the canonical procedure and minimizing the corresponding action [20], we obtain the equations of motion in the effective potential $U = \ln(\eta^2 D_{\rm s})$:

$$\ddot{q}_i = (\dot{q}_j \partial_j U)\dot{q}_i - \tfrac{1}{2}\dot{q}_j\dot{q}_j\partial_i U \tag{46}$$

where $q_1 = \xi$ and $q_2 = \eta$. Even if equation (46) is nonlinear with a friction term, one can show that the trajectory of extremal action between the centres of two neighbouring triangles follows the ridge of the surface $D_{\rm s}(\zeta)$.

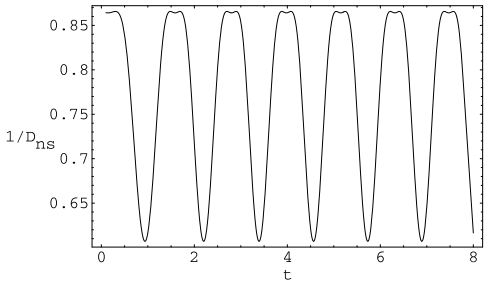

Figure 9. $D_{\rm ns}^{-1}$ running along a horocycle at constant velocity. Periodicity shows that the tree is isometric.

It is noteworthy that obtaining an analytical support of Cayley graphs is of great importance, since those graphs clearly display ultrametric properties and have connections to p-adic surfaces [21]. The detailed study of metric properties of the functions $D_{\rm s}^{-1}(\zeta)$ and $D_{\rm ns}^{-1}(\zeta)$ is left for separate publication.

While the self-similar properties of the Jacobians of those conformal mappings appear clearly in figure 8, one could wonder how the local symmetry breaking affects the continuous problem. We can see that if $D_{\rm s}^{-1}(\zeta)$ is univalued along the embedded tree, $D_{\rm ns}^{-1}(\zeta)$ does vary, which makes the tree locally non-uniform and leads to a multifractal behaviour. In other words, different paths of the same length along the tree have the same weights in the symmetric case, but have different ones in the non-symmetric case. The probability of a random path C of length L can be written in terms of a path integral with a Wiener measure

$$p_C = \mathcal{D}\{s\} \exp\left\{ -\int_0^L \frac{1}{D[s(t)]} \left(\frac{{\rm d}s}{{\rm d}t}\right)^2 {\rm d}t \right\} \tag{47}$$

where $s(t)$ is a parametric representation of the path C.

The first horocycles in figure 8 can be parametrized as follows:

$$\begin{aligned} \xi &= \tfrac{1}{2} \pm (\tfrac{1}{2} - \tfrac{1}{3}\sqrt{3}\sin\theta) \\ \eta &= \tfrac{1}{3}\sqrt{3}(1-\cos\theta) \end{aligned} \tag{48}$$

with θ running in the interval $[0, \pi/2]$. The condition ensuring the constant velocity $\dot{s} \equiv \frac{{\rm d}s}{{\rm d}t}$ along the horocycles gives with (41)

$$\frac{1}{\eta}\frac{{\rm d}\theta}{{\rm d}t} = \text{constant}$$

hence

$$\theta(t) = \arctan\left(\frac{1}{t}\right) \tag{49}$$

with a proper choice of the time unit. This parametrization is used to check that the embedded tree is isometric. Indeed, the horocycles shown in figure 8 correspond to a periodic sequence of steps like $\beta_1\beta_2\beta_1\beta_2\ldots$, $\beta_1\beta_3\beta_1\beta_3\ldots$ or $\beta_2\beta_3\beta_2\beta_3\ldots$. It is natural to assert that a step carries a Boltzmann weight characterized by the corresponding local values of $D_{\rm ns}^{-1}$. Therefore, the period of the plot shown in figure 9 is directly linked to the spacing of the tree embedded in the profile $D_{\rm ns}^{-1}$.

Coming back to the probability of different paths covered at constant velocity, one can write

$$-\log p_C \propto \int_{t_1}^{t_2} \frac{{\rm d}t}{D[s(t)]}. \tag{50}$$

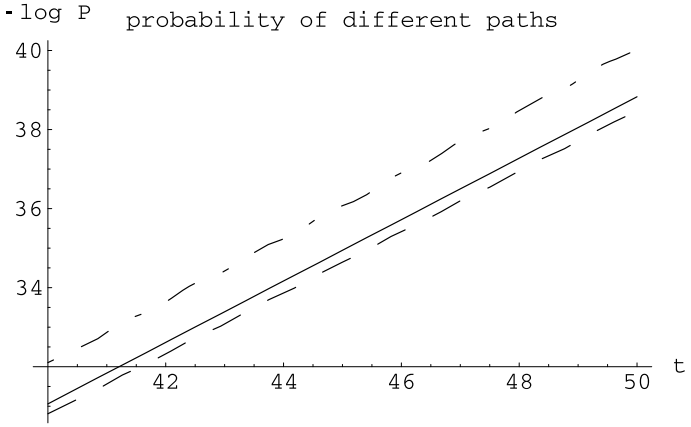

Figure 10. Probability of different paths along horocycles. Broken and chain curves correspond to right- and left-hand side horocycles on the non-symmetric surface, while the full line shows both right- and left-hand side horocycles on the symmetric surface.

Figure 10 shows the value $-\log p_C$ in symmetric and non-symmetric cases for different paths starting at $t_1 = 0^+$ and ending at t. In the symmetric case all plots are the same (full line), whereas in the non-symmetric case they are different: broken and chain lines display the corresponding plots for the sequences $\beta_2\beta_3\beta_2\beta_3\ldots$ and $\beta_1\beta_3\beta_1\beta_3\ldots$.

Following the outline of the construction of the fractal dimensions D_q given in section 2, we can describe multifractality in the continuous case by

$$D_q = -\frac{1}{q-1}\lim_{L\to\infty}\frac{1}{\ln \mathcal{N}(L)}\ln\frac{\int \mathcal{D}\{s\}\exp\left\{-q\int_0^L D_{\rm ns}^{-1}(s(t))\,\mathrm{d}t\right\}}{\left[\int \mathcal{D}\{s\}\exp\left\{-\int_0^L D_{\rm ns}^{-1}(s(t))\,\mathrm{d}t\right\}\right]^q} \tag{51}$$

where $\mathcal{N}(l)$ is the area of the surface covered by the trajectories of length L. This form is consistent with definitions (1) and (16). Indeed, if instead of the usual Wiener measure one chooses a discrete measure $\mathrm{d}\chi_T$, which is non-zero only for trajectories along the Cayley tree, we recover the following description.

Define the distribution function $\Theta(\beta_1,\beta_2,\beta_3,k) \equiv \Theta(\beta_1/\beta_3,\beta_2/\beta_3,k)$, which has the sense of a weighted number of directed paths of k steps on the non-symmetric three-branching Cayley tree shown in figure 7. The values of the effective Boltzmann weights β_1/β_3 and β_2/β_3 are defined in terms of the local heights of the surface $D_{\rm ns}^{-1}$ along the corresponding branches of the embedded tree. We set

$$\begin{aligned}\frac{\beta_1}{\beta_3} &= \exp\left[\int_{t_1}^{t_2}\frac{\mathrm{d}t}{D_{\rm ns}[s_r(t)]} - \int_{t_2}^{t_3}\frac{\mathrm{d}t}{D_{\rm ns}[s_r(t)]}\right] \approx 1.07\\ \frac{\beta_2}{\beta_3} &= \exp\left[\int_{t_1}^{t_2}\frac{\mathrm{d}t}{D_{\rm ns}[s_l(t)]} - \int_{t_2}^{t_3}\frac{\mathrm{d}t}{D_{\rm ns}[s_l(t)]}\right] \approx 1.19\end{aligned} \tag{52}$$

where t_1, t_2, t_3 are adjusted so that $s_r(t)$ represents a step weighted with β_3 for $t_1 < t < t_2$ and a step weighted with β_1 for $t_2 < t < t_3$ for right-hand side horocycles, while $s_l(t)$ represents a step weighted with β_3 for $t_1 < t < t_2$ and a step weighted with β_2 for $t_2 < t < t_3$ for left-hand side horocycles.

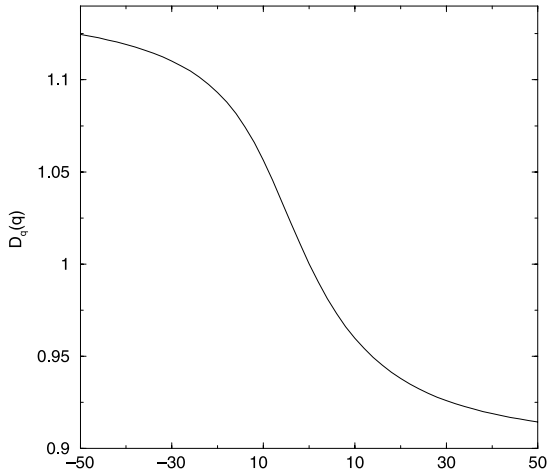

Figure 11. Multifractality of trajectories on a non-symmetric tree with Boltzmann weights defined by the Jacobian of the conformal mapping (45).

The partition function $\Theta\,(\beta_1/\beta_3, \beta_2/\beta_3, k)$ can be computed via a straightforward generalization of equation (9); it can be written in the form

$$\Theta\left(\frac{\beta_1}{\beta_3}, \frac{\beta_2}{\beta_3}, k\right) = A_0\lambda_1^{k-1} + B_0\lambda_2^{k-1} + C_0\lambda_3^{k-1} \qquad (k \geqslant 1) \tag{53}$$

where λ_1, λ_2 and λ_3 are the roots of the cubic equation

$$\lambda^3 - \lambda\left(1 + \frac{\beta_2^2}{\beta_3^2} + \frac{\beta_1\,\beta_2}{\beta_3^2}\right) - \left(\frac{\beta_1\,\beta_2}{\beta_3^2} + \frac{\beta_2^2}{\beta_3^2}\right) = 0$$

and A_0, B_0 and C_0 are the solutions of the following system of linear equations:

$$A_0 + B_0 + C_0 = 1 + \frac{\beta_1}{\beta_3} + \frac{\beta_2}{\beta_3}$$

$$A_0\lambda_1 + B_0\lambda_2 + C_0\lambda_3 = 2\frac{\beta_1}{\beta_3} + 2\frac{\beta_2}{\beta_3} + 2\frac{\beta_1\beta_2}{\beta_3^2}$$

$$A_0\lambda_1^2 + B_0\lambda_2^2 + C_0\lambda_3^2 = \frac{\beta_1}{\beta_3} + \frac{\beta_2}{\beta_3} + \frac{\beta_2^2}{\beta_3^2} + \frac{\beta_1^2}{\beta_3^2} + 6\frac{\beta_1\beta_2}{\beta_3^2} + \frac{\beta_1^2\beta_2}{\beta_3^3} + \frac{\beta_1\beta_2^2}{\beta_3^3}.$$

Knowing the distribution function $\Theta\,(\beta_1/\beta_3, \beta_2/\beta_3, k)$, equation (51) with the discrete measure $\mathrm{d}\chi_T$ now reads (compare with (16) and (17))

$$D_q = -\frac{1}{q-1}\lim_{k\to\infty}\frac{\ln\Theta\,([\beta_1/\beta_3]^q\,, [\beta_2/\beta_3]^q\,, k) - q\ln\Theta\,(\beta_1/\beta_3, \beta_2/\beta_3, k)}{\ln(3\times 2^{k-1})}. \tag{54}$$

The plot of the function $D_q(q)$ is shown in figure 11 (the plot is drawn for $k = 100\,000$).

5. Discussion

The results presented in sections 2–4 are summarized; they underline several problems still unsolved related to our work, and raise the issue of their possible applications to real physical systems.

(a) The basic concepts of multifractality have been clearly formulated mainly for abstract systems in [1]. In this paper, we have tried to remain as close as possible to these classical formulations, while adding to abstract models of [1] the new physical content of topological properties of random walks entangled with an array of obstacles. Our results point out two conditions which generate multifractality for any physical system: (i) an exponentially growing number of states, i.e. 'hyperbolicity' of the phase space and (ii) the breaking of a local symmetry of the phase space (while on large scales the phase space could remain isotropic).

In section 2 we have considered the topological properties of the discrete 'random walk in a rectangular lattice of obstacles' model. Generalizing an approach developed earlier (see, for example, [13] and references therein) we have shown that the topological phase space of the model is a Cayley tree whose associated transition probabilities are non-symmetric. Transition probabilities have been computed from the basic characteristics of a free random walk within the elementary cell of the lattice of obstacles. The family of generalized Hausdorff dimensions $D_q(q)$ for the partition function $\Omega(\beta^q, k)$ (where k is the distance on the Cayley graph which parametrizes the topological state of the trajectory) exhibits a non-trivial dependence on q, which means that different moments of the partition function $\Omega(\beta^q, k)$ scale in different ways, for example, such that $\Omega(\beta^q, k)$ is multifractal.

The main topologically probabilistic issues concerning the distribution of random walks in a rectangular lattice of obstacles have been considered in section 3. In particular, we have computed the average 'degree of entanglement' of an $\tilde{N}$-step random walk and the probability for an $\tilde{N}$-step random walk to be closed and unentangled. Results have been achieved through a renormalization-group technique on a non-symmetric Cayley tree. The renormalization procedure has allowed us to overcome one major difficulty: in spite of a locally broken spherical symmetry, we have mapped our problem to a symmetric random walk on a tree of effective branching number z depending on the lattice parameters. To validate our procedure, we have compared the return probabilities obtained via our RG approach with the exact result of Gerl and Woess [15] and found a very good numerical agreement.

The problem tackled in section 4 is closely related to that discussed in section 2. We believe that the approach developed in section 4 could be very important and informative as it explicitly shows that multifractality is not attached to particular properties of a statistical system (such as random walks in our case) but deals directly with metric properties of the topological phase space. As we have already pointed out, the required conformal transforms are known only for triangular lattices, what restricts our study. However, we showed explicitly that the transform $z_{\rm ns}(\zeta)$ maps the multi-punctured complex plane z onto the so-called 'topological phase space', which is the complex plane ζ free of topological obstacles (all obstacles are mapped onto the real axis). We have connected multifractality to the multi-valley structure of the properly normalized Jacobian $D_{\rm ns}(\xi, \eta)$ of the non-symmetric conformal mapping $z_{ns}(\zeta)$. The conformal mapping obtained has deep relations with number theory, which we are going to discuss in a forthcoming publication.

(b) The 'random walk in an array of obstacles' model can be considered as a basis of a mean-field-like approach to the problem of entropy calculations in sets of strongly entangled fluctuating polymer chains. Namely, we choose a test chain, specify its topological state and assume that the lattice of obstacles models the effect of entanglements with the surrounding chains (the 'background'). Changing c_x and c_y one can mimic the affine deformation of the background. Investigating the free energy of the test chain entangled

with the deformed media is an important step towards understanding the high elasticity of polymeric rubbers [11].

Neglecting the fluctuations of the background as well as the topological constraints which the test chain produces by itself leads to information loss concerning the correlations between the test chain and the background. Yet, even in this simplest case we obtain non-trivial statistical results concerning the test chain topologically interacting with the background.

The first attempts to go beyond the mean-field approximation of the RWAO model and to develop a microscopic approach to the statistics of mutually entangled chain-like objects have been undertaken recently in [22]. We believe that investigating multifractality of such systems is worthy of attention.

Acknowledgments

The authors are grateful to A Comtet for valuable discussions and helpful comments, and would like to thank the referees for drawing their attention to references [23–25].

References

[1] Halsey T, Jensen M, Kadanoff L, Procaccia I and Shraiman B 1986 *Phys. Rev.* A **33** 1141
[2] Stanley H and Meakin P 1988 *Nature* **335** 405
[3] Arneodo A, Grasseau G and Holschneider M 1988 *Phys. Rev. Lett.* **61** 2281
[4] Duplantier B 1999 *Phys. Rev. Lett.* **82** 469
(Duplantier B 1999 *Preprint* cond-mat/9901008)
[5] Kogan I, Mudry C and Tsvelik A 1996 *Phys. Rev. Lett.* **77** 707
Caux J, Kogan I and Tsvelik A 1996 *Nucl. Phys.* B **466** 444
[6] Chamon C, Mudry C and Wen X 1996 *Phys. Rev. Lett.* **77** 4196
[7] Castillo H, Chamon C, Fradkin E, Goldbart P and Mudry C 1997 *Phys. Rev.* B **56** 10668
[8] Derrida B and Spohn H 1988 *J. Stat. Phys.* **51** 817
[9] Pesin Ya and Weiss H 1997 *Chaos* **7** 89
[10] Nechaev S and Khokhlov A R 1985 *Phys. Lett.* A **112** 156
Nechaev S, Semenov A N and Koleva M K 1987 *Physica* A **140** 506
[11] Khokhlov A R and Ternovskii F F 1986 *Sov. Phys.–JETP* **63** 728
Khokhlov A R, Ternovskii F F and Zheligovskaya E A 1990 *Physica* A **163** 747
[12] Helfand E and Pearson D 1983 *J. Chem. Phys.* **79** 2054
Helfand E and Rubinstein M 1985 *J. Chem. Phys.* **82** 2477
[13] Nechaev S 1998 *Sov. Phys.–Usp.* **41** 313
Nechaev S 1999 *Topological Aspects of Low Dimensional Systems (Les Houches 1998)* (Berlin: Springer)
(Nechaev S 1998 *Preprint* cond-mat/9812205)
[14] Kesten H 1959 *Trans. Am. Math. Soc.* **92** 336
[15] Gerl P and Woess W 1986 *Probab. Theor. Rel. Fields* **71** 341
[16] Woess W 1994 *Bull. London Math. Soc.* **26**
[17] Koppenfels W and Stalman F 1959 *Praxis der Konformen Abbildung* (Berlin: Springer)
Kober H 1957 *Dictionary of Conformal Representation* (New York: Dover)
[18] Ito K and McKean H P 1965 *Diffusion Processes and Their Sample Paths* (Berlin: Springer)
[19] Abramowitz M and Stegun I 1964 *Handbook on Mathematical Functions* (Washington, DC: US Govt Printing Office)
[20] Feynman R and Hibbs A R 1965 *Quantum Mechanics and Path Integrals* (New York: McGraw-Hill)
[21] Brekke L and Freund P 1993 *Phys. Rep.* **233** 1
[22] Desbois J and Nechaev S 1998 *J. Phys. A: Math. Gen.* **31** 2767
Vershik A, Nechaev S and Bikbov R 2000 *Commun. Math. Phys.* **212** 469
Vershik A 2000 *Russ. Math. Surv.* to appear
[23] Lyons R 1992 *Ann. Probab.* **20** 125
[24] Lyons R and Pemantle R 1992 *Ann. Probab.* **18** 931
[25] Holley R and Waymire E 1992 *Ann. App. Probab.* **2** 819